REPORT DOCUMENTATION PAGE

Form Approved
OMB No. 0704-0188

1. REPORT DATE *(DD-MM-YYYY)*	2. REPORT TYPE	3. DATES COVERED *(From - To)*
05-04-2013	Journal Article	

4. TITLE AND SUBTITLE

Impacts of Underwater Turbulence on Acoustical and Optical Signals and Their Linkage

5a. CONTRACT NUMBER

5b. GRANT NUMBER

5c. PROGRAM ELEMENT NUMBER

0602782N

6. AUTHOR(S)

Weilin Hou, Ewa Jarosz, Sarah Woods, Wesley Goode and Alan Weidemann

5d. PROJECT NUMBER

5e. TASK NUMBER

5f. WORK UNIT NUMBER

73-6369-01-5

7. PERFORMING ORGANIZATION NAME(S) AND ADDRESS(ES)

Naval Research Laboratory
Oceanography Division
Stennis Space Center, MS 39529-5004

8. PERFORMING ORGANIZATION REPORT NUMBER

NRL/JA/7330--11-0750

9. SPONSORING/MONITORING AGENCY NAME(S) AND ADDRESS(ES)

Office of Naval Research
One Liberty Center
875 North Randolph Street, Suite 1425
Arlington, VA 22203-1995

10. SPONSOR/MONITOR'S ACRONYM(S)

ONR

11. SPONSOR/MONITOR'S REPORT NUMBER(S)

12. DISTRIBUTION/AVAILABILITY STATEMENT

Approved for public release, distribution is unlimited.

13. SUPPLEMENTARY NOTES

14. ABSTRACT

Acoustical and optical signal transmission underwater is of vital interest for both civilian and military applications. The range and signal to noise during the transmission, as a function of system and water optical properties, in terms of absorption and scattering, determines the effectiveness of deployed electro-optical (EO) technology. The impacts from turbulence have been demonstrated to affect system performance comparable to those from particles by recent studies. This paper examines the impacts from underwater turbulence on both acoustic scattering and EO imaging degradation, and establishes a framework that can be used to correlate these. It is hypothesized here that underwater turbulence would influence the acoustic scattering cross section and the optical turbulence intensity coefficient in a similar manner. Data from a recent field campaign, Skaneateles Optical Turbulence Exercise (SOTEX, July, 2010) is used to examine the above relationship. Results presented here show strong correlation between the acoustic scattering cross-sections and the intensity coefficient related to the modulation transfer function of an EO imaging system. This significant finding will pave ways to utilize long range acoustical returns to predict EO system performance.

15. SUBJECT TERMS

oceanic optics, optical transfer functions, spatial resolution, turbulence, visability and imaging

16. SECURITY CLASSIFICATION OF:			17. LIMITATION OF ABSTRACT	18. NUMBER OF PAGES	19a. NAME OF RESPONSIBLE PERSON
a. REPORT	b. ABSTRACT	c. THIS PAGE			Weilin Hou
Unclassified	Unclassified	Unclassified	UU	9	19b. TELEPHONE NUMBER *(Include area code)* 228-688-5257

14. P. C. Chang, J. C. Flitton, K. I. Hopcraft, E. Jakeman, D. L. Jordan, and J. G. Walker, "Improving visibility depth in passive underwater imaging by use of polarization," Appl. Opt. **42**(15), 2794–2803 (2003).
15. L. Mullen, A. Laux, B. M. Concannon, E. P. Zege, I. L. Katsev, and A. S. Prikhach, "Amplitude-modulated laser imager," Appl. Opt. **43**(19), 3874–3892 (2004).
16. G. R. Fournier, D. Bonnier, J. L. Forand, and P. W. Pace, "Range-gated underwater laser imaging system," Opt. Eng. **32**(9), 2185 (1993).
17. D. Sadot, A. Dvir, I. Bergel, and N. Kopeika, "Restoration of thermal Images distorted by the atmosphere, based on measured and theoretical atmospheric modulation transfer function," Opt. Eng. **33**, 44–53 (1994).
18. Y. Yitzhaky, I. Dror, and N. Kopeika, "Restoration of atmospherically blurred images according to weather-predicted atmospheric modulation transfer functions," Opt. Eng. **36**(11), 3064–3072 (1997).
19. D. J. Bogucki, J. A. Domaradzki, R. E. Ecke, and C. R. Truman, "Light scattering on oceanic turbulence," Appl. Opt. **43**(30), 5662–5668 (2004).
20. J. W. Goodman, *Statistical Optics* (John Wiley & Sons, 1985).
21. T. Ross and R. Lueck, "Sound scattering from oceanic turbulence," Geophys. Res. Lett. **30**(6), 1343 (2003).
22. S. Woods, W. Hou, W. Goode, E. Jarosz, and A. Weidemann, "Quantifying turbulence microstructure for improvement of underwater Imaging," in *Ocean Sensing and Monitoring, SPIE Defense and Security Symposium*, W. Hou, ed. (SPIE, Orlando, FL, 2011).
23. S. W. Effler, A. R. Rrestigiacomo, and D. M. O'Donnel, "Water quality and limonological monitoring for Skaneateles Lake: Field Year 2007," (Upstate Freshwater Institute, 2008), p. 57.
24. T. R. Osborn and C. S. Cox, "Oceanic fine structure," Geophys. Astrophys. Fluid Dyn. **3**(1), 321–345 (1972).
25. G. K. Batchelor, "Small-scale variation of convected quantities like temperature in turbulence fluid," J. Fluid Mech. **5**, 113–133 (1959).
26. J. W. Goodman, *Introduction to Fourier Optics* (Roberts & Company Publishers, 2005).

1. Introduction

Diver visibility has been one of the key research areas in underwater vision and imaging studies. Its applications also extend into imaging system performance evaluation and prediction, which is important in mine warfare (MIW) and anti-submarine warfare (ASW) operations. These could include diver visibility, search and rescue, mine detection and identification, as well as optical communications. These applications are often associated with coastal ocean waters, and this is generally translated directly into turbidity of the water column [1–3]. While this is typically the case, exceptions can lead to erroneous predictions and decisions, including dispatching of search and rescue assets in un-operational regions [4]. One of these exceptions is the impact from underwater turbulence. As the strength of electro-optical (EO) systems lies in their high resolution and associated albedo and texture for identification, the reduction in resolution in underwater environments strongly limits their applicability in both civilian and military scenarios. The image quality degradation of EO systems in underwater environments has been almost exclusively examined from impacts of particulates in the water, even though evidence from earlier studies has shown the possibility of strong degradation from turbulence, especially in clean waters [5–7]. This important element is currently under-studied in research and system development, as early results showed that high resolution details, which correspond to high spatial frequencies, are precisely what optical turbulence impacts the most [8, 9].

Better understanding of the process, and more importantly, developing means to quantify these impacts, is a crucial research element that will benefit the above mentioned visibility applications. One of the issues that hinder the research is to identifying and implementing ways to effectively quantify underwater turbulence structures. The traditional approach to quantify the turbulence structure involves spot sampling techniques with either acoustical scattering properties such as those relying on Doppler effects, or mechanical means involving Piezo electric derived shear probes. While these methods provide the most reliable, direct and accurate assessment to-date, they do not offer the capability of synoptic coverage over distance, nor instantaneous measurements over the light path, which is vital in assessing total impacts on EO signal transmission. One possible solution is to use the scattering properties of the acoustical signal over these microstructures [10, 11], as acoustical signals do provide coverage over longer range, while encountering the same impacts as optical signals.

#183363 - $15.00 USD Received 11 Jan 2013; accepted 14 Jan 2013; published 12 Feb 2013

2. Theoretical background

When it comes to diver visibility, the most prominent issue is the degradation of image quality over distance due to scattering in water. This presents a striking contrast for those of us who are accustomed to the seemingly unlimited visual ranges in air. The cause of the degradation has been mostly attributed to the particles of various origins in the water and it is rightly so. Most research has been focused on reducing the impact of particle scattering by means of discriminating scattering photons involving polarization, range gating, modulation, and by means of restoration via deconvolution [1, 12–16]. However, in certain oceanic or lake waters, another factor could come into play. This is the scattering by optical turbulence, which is the result of the variations of the index of refraction of the medium. This scattering is mostly associated with the turbulence structures of the medium, or water body in our case. Degradation of the image quality in a scattering medium involving turbulence has been studied mostly in the atmosphere. These studies are mainly focused on modeling the optical transfer function (OTF), in an effort to restore the images obtained, such as in air reconnaissance or astronomy studies [17, 18]. Similar effects of underwater turbulence have been postulated to have impacts over long image transmission range [5], which has been supported by light scattering measurements and simulations [19]. Under extreme conditions, observations have been made that involves targets with a pathlength of only a few feet [6]. The images obtained under such conditions are often severely degraded or blurred, on par with or more than those caused by particle scattering. A simple underwater imaging model, or SUIM [9], was developed to address this issue and it has been shown that, on average, the relative contribution of different components [1, 2], namely, path radiance, particle and turbulence scattering, in underwater imaging applications can be expressed in terms of the OTF as

$$\begin{aligned} OTF(\psi,r)_{total} &= OTF(\psi,r)_{path} OTF(\psi,r)_{par} OTF(\psi,r)_{tur} \\ &= \left(\frac{1}{1+D}\right)\exp\left[-cr + br\left(\frac{1-e^{-2\pi\theta_0\psi}}{2\pi\theta_0\psi}\right)\right]\exp\left(-S_n\psi^{5/3}r\right) \\ &= \left(\frac{1}{1+D}\right)\exp\left\{-\left[c - b\left(\frac{1-e^{-2\pi\theta_0\psi}}{2\pi\theta_0\psi}\right) + S_n\psi^{5/3}\right]r\right\} \end{aligned} \tag{1}$$

where θ_0 relates to the mean scattering angle, c and b are the beam attenuation and scattering coefficients respectively. Ψ is the spatial frequency in cycles per radian, r is the imaging range, and D relates to path radiance. S_n is defined as the optical turbulence intensity coefficient, and contains parameters that are dependent on the structure function [20], which can be further expressed as a function of the turbulence dissipation rates of temperature, salinity and kinetic energy, assuming Kolmogorov type power spectrum. For convenience, it is rewritten here as

$$S_n = 3.44(\overline{\lambda}/R_0)^{5/3} = 1736K_3\overline{\lambda}^{1/3} \tag{2}$$

where K_3=$B_1\chi\varepsilon^{-1/3}$, and reflects the 3-dimensional optical turbulence strength. $\overline{\lambda}$ is the average wavelength of the transmitted light. R_0 is the characteristic seeing parameter. B_1 is a constant, and assumed to be on the order of unity. The kinetic energy dissipation rate (TKED, ε), typically ranges from 10^{-3} to 10^{-11} m^2s^{-3} in natural waters. χ relates to the dissipation rate of temperature (TD) or salinity variances [9].

Since the phase information can be ignored under incoherent imaging conditions, the magnitude of the OTF or the modulation transfer function (MTF) will be used interchangeably here. The above model has been validated using both direct and indirect field

#183363 - $15.00 USD
Received 11 Jan 2013; accepted 14 Jan 2013; published 12 Feb 2013

measurements [8, 9], and S_n can be used as a proxy for optical turbulence intensity that relates directly with image quality degradation.

We argue that the same turbulent microstructures in the ocean could impact the sound propagation and scattering in a somewhat similar manner, despite the differences in pressure versus electromagnetic waves. The turbulence scattering cross-section (σ) for a given sound frequency has been shown to be proportional to the first order derivatives of the one dimensional spectrum $\phi(k)$ of the sound speed fluctuations [11, 21], namely

$$\sigma = C_1 \frac{-k_z^3}{2} \frac{d\Phi_T(k_z)}{dk_z}. \quad (3)$$

A simplified form is used here as we opt to neglect the contribution from salinity for the time being, as data from a freshwater lake will be used, and assume $\Phi = \Phi_T$ (temperature only, omitting subscript T hereon). C_1 denotes a numerical constant. The spectrum can be further expressed as a function of k_z (vertical wavenumber), ε, χ, in a combined spectra including buoyancy-dominated, inertial and Batchelor subranges [11]

$$\Phi(k_z) = C_2[N^2\chi\varepsilon^{-1}k_z^{-3} + B_1\chi\varepsilon^{-1/3}k_z^{-5/3} + \chi\left(\frac{\varepsilon}{\nu}\right)^{1/2} k_z^{-1}]\exp[-q\left(\frac{k_z}{k_B}\right)^2], \quad (4)$$

where k_B is the diffusive cutoff wavenumber, associated with the Batchelor subrange boundary, as [22]:

$$k_B = \left(\frac{1}{2\pi}\right)\left(\frac{\varepsilon}{\nu D_T^2}\right)^{0.25} \quad (5)$$

ν and D_T denote the kinematic viscosity and thermal diffusivity of seawater respectively. N is the buoyancy frequency, q and C_2 are numerical constants.

3. Field exercise

3.1 Setup

From above analysis, one could expect to see a meaningful relationship between S_n and σ as expressed in Eqs. (2) and (3). We set out to obtain field data to examine image degradation as a function of the microstructure turbulence. As underwater optical turbulence is primarily a function of the temperature structure, intensified thermoclines in natural environments provide a convenient setup to examine this chaotic process. We thus identified one of the finger lakes in upstate New York, Skaneateles, as our test site for SOTEX (Skaneateles Optical Turbulence EXercise, July, 2010). Figure 1(a) shows the approximate location of the two sampling stations, the first (S1, red circle) near the center of the lake (42.8668° N, 76.3920° W) over a sloping bottom with an approximate depth of 70m, and the second (S2, blue triangle) at the northern end of the lake (42.9063° N, 76.4058° W) over a flatter bottom with an approximate depth of 50m. The lake is the clearest of all the Finger Lakes, with an average Secchi depth near 8 to 12 m [23], or beam attenuation values less than $0.4m^{-1}$ for 532nm in most cases [8], and allowed for imaging under varied turbulent strength, with little scattering contribution from particulates. The strong stratification in July at relatively shallow depth, and low wind and current interference ensure a well-defined thermocline, as demonstrated by the temperature profiles shown in Fig. 1(b). The same features help to form strong structures for optical turbulence in the lake. The optical properties of the water column were measured with a 9-channel absorption and attenuation meter (ac-9, WETLabs), and Laser In Situ Scattering Transmissometer (LISST, Sequoia Scientific).

#183363 - $15.00 USD
Received 11 Jan 2013; accepted 14 Jan 2013; published 12 Feb 2013

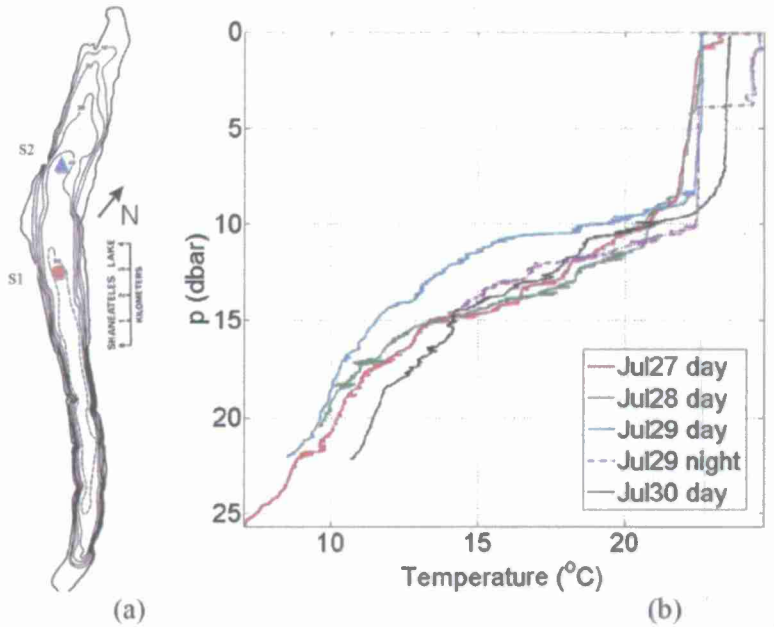

Fig. 1. **(left, a)** Bathymetric sketch of Skaneateles Lake showing the approximate location of the two stations: S1 (red circle) near the center of the lake, and S2 (blue triangle) in the northern end of the lake. Map from http://www.ourlake.org/html/skaneateles_lake1.html. **(right, b)** Temperature profiles corresponding to the dissipation profiles shown in Fig. 2-6 for deployments on July 27 day (solid red), July 28 day (solid green), July 29 day (solid blue), July 29 night (dashed purple), July 30 day (solid black). All profiles are from S1 except for the July 29th daytime deployment, which is from S2.

Turbulence measurements of the water column were carried out by a Vertical Microstructure Profiler (VMP, Rockland Scientific), a 3D acoustic Doppler velocimeter (Vector, Nortek), and a Precision Measurements Engineering (PME) fast Conductivity and Temperature (CT) sensor. To estimate the effects of the optical turbulence in the water column, it is essential to remove any other variations that could contribute to the blurring of the imagery obtained. For this reason, the Image Measurement Assembly for Subsurface Turbulence (IMAST) was designed. The camera and housing, and passive and active imaging targets were attached to a 5m rigid aluminum structure, along with the velocimeter, and a CTD. The two instruments, Vector and CT, are mounted near the center of the IMAST structure, and the heads of the instruments placed in such a way as to sample the same volume of water, thus providing time series of the 3D velocity, temperature, and conductivity fluctuations of the sample water volume. As the two instruments (Vector/CT) are commonly used for laboratory measurements or stationary moorings, the setup requires collection of a time series of velocities at a stationary depth in order to compute the turbulent dissipation rates. Therefore, during deployment, the IMAST profiled the water column by pausing at each depth for ten to fifteen minutes to capture the turbulence statistics.

The VMP profiler, designed to measure microstructures in oceans and lakes up to 500 m, is used to profile the water column for vertical structures. It is equipped with four microstructure sensors: two current shear sensors, one thermistor (FP07), and a micro-conductivity sensor (SBE7). These sensors allow measuring with high accuracy and resolution microscale velocity shear, temperature, and conductivity. Additionally, the VMP profiler has externally attached SeaBird SBE7-3F temperature and SBE-4C conductivity

#183363 - $15.00 USD
Received 11 Jan 2013; accepted 14 Jan 2013; published 12 Feb 2013

sensors. The profiler also measures pressure and provides dissipation rates as a function of depth.

This allows two different measurement approaches, namely the shear-probe-based, and acoustical-Doppler-based to be compared. Initial results showed comparable TKED dissipation rates between the two configurations [22]. These provide needed validation amongst our instrumentation setup. We consider the VMP data to be validated in this sense and only VMP data will be used in exploring the relationship for the profile comparison in the following sections.

3.2 VMP turbulence measurements and calculations

During the SOTEX experiment, over 100 VMP profiles were executed and used to estimate turbulent energy (shear data) and temperature (thermistor data) dissipation rates. The turbulent energy dissipation rate, ε, was computed by integrating the shear spectrum from k_1 to k_2 using the isotropic formula:

$$\varepsilon = \frac{15}{2} \nu \int_{k_1}^{k_2} \varphi(k)\, dk \tag{6}$$

where k is the wavenumber, ν is the kinematic molecular viscosity of water, and φ(k) is the shear spectrum. Spectra of the velocity shear were calculated from consecutive segments of 1024 data points, corresponding to a bin height of approximately 0.8 m, with an overlap between adjacent bins of 512 points. The lowest wavenumber k_1 was set to 1 cpm, and the highest one (k_2) was set to the wavenumber where the shear spectrum has a minimum between the natural spectrum and a high wavenumber peak, but not higher than 30 cpm due to signal to noise levels. Different profiling velocities were employed in order to better quantify dissipation rates of TKED (~70 cm/s) and TD (~30cm/s).

The rate of loss of temperature variance is determined from microstructure measurements of temperature using the very fast-response (glass-enclosed) thermistors. Assuming isotropy, the thermal dissipation rate, χ_T, was estimated following the below formula [24]:

$$\chi_T = 6 D_T \overline{\left(\frac{dT'}{dz} \right)^2} \tag{7}$$

where T' is the temperature fluctuation, and $\overline{\left(\frac{dT'}{dz} \right)^2}$ is the bin average of the squared gradient of the temperature variance in the vertical direction, z. An accurate determination of χ_T requires estimates of spatial temperature gradients with resolution to the Batchelor scale, which is beyond the capability of conventional sensors. Hence, interpolation was made for SOTEX observations by fitting the measured temperature gradient spectra determined over a limited wavenumber range to the universal Batchelor form [25]. The cutoff wavenumber is as defined in Eq. (5). Spectra of the temperature gradient were calculated from consecutive segments of 1024 data points with an overlap between adjacent bins of 512 points, corresponding to a mean bin height of approximately 0.45 m.

Sample results from different days can be seen in Figs. 2-3. These are dissipation rate profiles of TKED (ε) and TD (χ, again, for convenience, subscript T is omitted), optical turbulence intensity coefficient (S_n) and acoustical scattering cross section (σ). The units for ε are $m^2 s^{-3}$, while those for χ are $°C^2 s^{-1}$. Since the main concern here is to examine the relative contribution and correlation between S_n and σ, they are not calibrated and therefore have arbitary units, and are offset by a constant value. Our focus here is to explore the shape of the profiles and examine their correlation, therefore the relative units are acceptable. On the other

#183363 - $15.00 USD
Received 11 Jan 2013; accepted 14 Jan 2013; published 12 Feb 2013

hand, these values will be offset by a constant in most cases, since they are all dependent upon the sound frequencies in consideration. Nonetheless, the general trend should still hold.

This is indeed the case by examining these figures. One should notice that the general trend of stronger turbulence at or near the thermocline around 10 to 15m, as shown by Fig. 1(b). The strong turbulence layer can be observed in both the TKED and TD rates throughout the exercise. It is encouraging, while not surprising, to see that indeed both the optical turbulence intensity coefficient (S_n), as well as the acoustic scattering cross section (σ), follow the same trend, shown in lower part of Figs. 2-3. As one can observe, this trend is predominantely determined by the temperature dissipation rate structure. This is in part due to the fact that this is a freshwater lake, and thus sound speed is affected by little, if any, conductivity variations. It is reasonable to believe such relationship still holds in the oceanic environment, as the extra term associated with salinity variations to be added in Eq. (3) is similar to the cascade properties of the MTF in Eq. (2) [26]. An oceanic research cruise has been scheduled to further test this relationship.

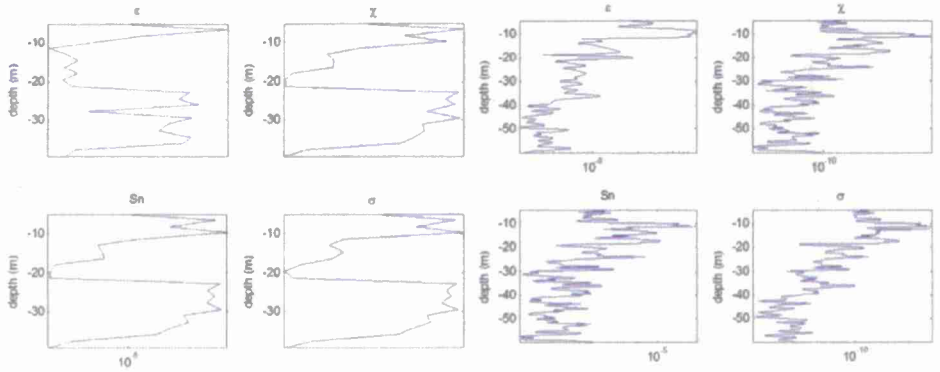

Fig. 2. VMP profiles of TKED (ε) and TD rates (χ), optical turbulence intensity (S_n) and acoustical scattering cross section (σ) on July 29, 2010 (Profile#62, **left**), on July 30, 2010 (Profile#112, **right**). The units for ε is m^2s^{-3}, while χ is $°C^2s^{-1}$. S_n and σ are not calibrated.

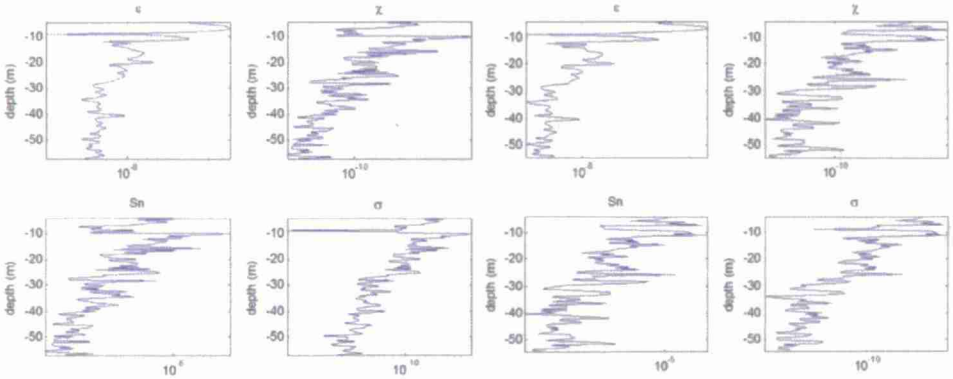

Fig. 3. VMP profiles of TKED (ε) and TD rates (χ), optical turbulence intensity (S_n) and acoustical scattering cross section (σ) on July 30, 2010 (Profile#117, **left**), on July 30, 2010 (Profile#126, **right**). The units for ε are m^2s^{-3}, while χ is C^2s^{-1}. S_n and σ are not calibrated.

The closely related trend observed from Figs. 2-3 is more obvious when S_n is plotted against σ in Figs. 4-6, and correlation coefficients are calculated. These graphs support our hypothesis about the positive relationship between the optical turbulence intensity and acoustic scattering cross sections by high degree of correlation coefficients, ranging from 0.86

#183363 - $15.00 USD
Received 11 Jan 2013; accepted 14 Jan 2013; published 12 Feb 2013

to 0.99 using log-log scales. The level of high correlation maintains, when all data points from these deployments are put on the same graph (Fig. 6). It is natural to see correlation suffer when sample space increase, especially when outliers from extreme events (natural due to noise issues; or artificial due to data processing) are likely to be included. The decreasing variance in the acoustical to optical relationship at higher turbulence intensity seems to support this argument further, due to higher signal to noise ratio at higher dissipation rates, as shown by Fig. 6. The result shown here supports a strong relationship between the optics and acoustics when strong turbulence present. It is worth mentioning that due to differences in deployment requirements, in order to quantify dissipation rates of TKED and TD, profiles have been interpolated to the nearest grids in space and time, in order to have co-incidental measurements at desired depth to quantify impacts on both optics and acoustics. This procedure would likely introduce undesired variances presented in figures. Efforts are underway to investigate and minimize these noise terms.

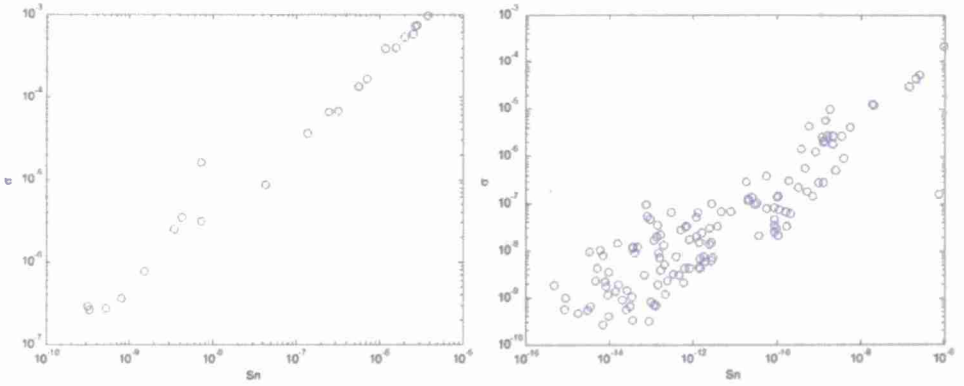

Fig. 4. Optical turbulence intensity (S_n) versus acoustical scattering cross section (σ) for July 29, 2010 (Profile#62, $R^2 = 0.99$, **left**), for July 30, 2010 (Profile#112, $R^2 = 0.89$, **right**)

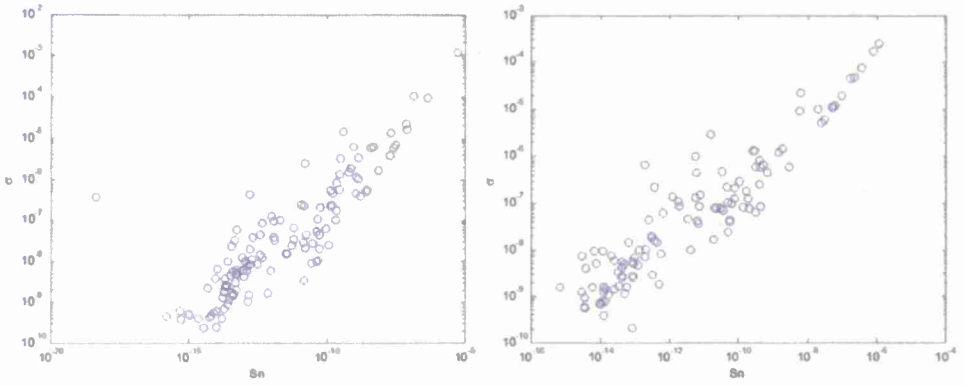

Fig. 5. Optical turbulence intensity (S_n) versus acoustical scattering cross section (σ), for July 30, 2010 (Profile#126, $R^2 = 0.93$, **left**), for July 30, 2010 (Profile#117, $R^2 = 0.86$, **right**)

#183363 - $15.00 USD
Received 11 Jan 2013; accepted 14 Jan 2013; published 12 Feb 2013

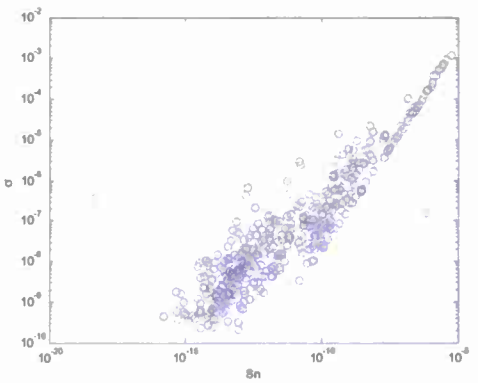

Fig. 6. Optical turbulence intensity (S_n) versus acoustical scattering cross section (σ), for July 28-30, 2010 (Profile#43, 75, 112, 126, $R^2 = 0.91$).

4. Summary

We established a practical approach to estimate optical signal degradation by utilizing acoustic scattering returns. This relationship is validated using data obtained during SOTEX. A strong correlation (>0.9) can be seen during multi-profile observations. Further validation is necessary, especially in more energetic, oceanic environments, where salinity variation will also contribute to the scattering returns in both acoustical and optical signals. Nevertheless, our results are very encouraging as it enables us to use long range acoustical signals to effectively predict optical system performance, especially those involving longer reach active systems in MIW and ASW applications. The impacts of turbulence on underwater imaging is a challenging topic that is important in understanding both physical environment parameterizations as well as diver visibility, including active and passive imaging system performance. When combined with current active EO imaging system performance model for Navy's mine hunting systems, this result enables us to significantly enhance prediction accuracy, as it addresses contributions from turbulence over long ranges, on top of particle contributions, for the first time.

#183363 - $15.00 USD
Received 11 Jan 2013; accepted 14 Jan 2013; published 12 Feb 2013